Polarimetric Scattering from a 3-D Rectangular Crack in a PEC Covered by a Dielectric Layer

Mehdi Bozorgi and Ahad Tavakoli

Electrical Engineering Department
Amirkabir University of Technology, Tehran, 15914, Iran
Mehdi_Bozorgi@aut.ac.ir, Tavakoli@aut.ac.ir

Abstract **─**A novel direct approach for calculation of the polarimetric scattering fields from a narrow 3-D rectangular crack in an infinite ground plane underneath a dielectric layer is presented. Since the electromagnetic fields are directly calculated and thus the approach in inversible, this technique is suitable for microwave NDT applications where cracks of narrow width, arbitrary length and depth under a dielectric layer are frequently encountered. A set of coupled field integral equations (FIE) with logarithmic and hypersingular kernels are derived and then descritized by a collocation method based on Chebyshev polynomials. The results of this direct approach are in good agreement with non-inversible full numerical FEM and MoM results.

Index Terms **─** 3-D rectangular crack, Chebyshev polynomials, dielectric layer, integral equation, and polarimetric scattering.

I. INTRODUCTION

To detect surface cracks in metals, several electromagnetic techniques are suggested [1-5]. Recently, far field polarimetric scattering measurements are proposed where common NDT techniques may not be practical such as in blast furnaces [6]. Oil, paint, electrical, and thermal coatings on cracks alters the scattering signature. For practical purposes, a solution that takes the dielectric coating effect into consideration is in demand.

Electromagnetic scattering from a dielectric coated slot in conductors is an ongoing research using various computational techniques. Initially, Knops and Cohn studied the effects of a dielectric layer on top of an aperture [7]. Later, Chen solved the integral equation for a waveguide ended with a dielectric slab and provided some physical and mathematical explanations [8]. Nevels and Butler used electric vector potential and Somerfeld integrals to model the diffraction from a slot covered by a dielectric layer [9-10]. Electromagnetic problems are generally formulated by means of the electric and the magnetic potential integral equations (PIE) [11-13]. Weak singularity of the Green's function allows utilization of a variety of numerical methods [14]. On the contrary, the electric field integral equations (EFIE) and the magnetic field integral equations (MFIE) have strong second-order singularity. Hadamard introduced the hypersingular integrals for solving Cauchy's hyperbolic partial differential problems as the finite part of a divergent integral [15]. An exact solution of the Hadamard integrals exists only in particular cases, where the hypersingular integrals are solved by approximate methods. One approach is transformation of the hypersingular integrals into singular or weakly singular integrals by various regularization techniques [16-18]. Another method that avoids singular point restrictions is the direct numerical computation of the finite part integrals by a variety of quadrature techniques.

Recently, in applied mathematics, some innovative methods are suggested to solve high order singular integrals effectively [19-20]. Thus, a strong singular EFIE or MFIE can be solved directly without using potential vectors and consequently, some tedious numerical computations such as the curl operator are eliminated. Here, an efficient approach based on finite part sense integrals is developed for calculation of electromagnetic scattering from a dielectric coated three-dimensional crack in a grounded slab.

In Section II, a set of coupled integral equations are formulated via the continuity of the tangential magnetic fields. In Section III, the calculation of the green's functions and in Section IV, the extraction of the singular terms leaving an integrable equation is presented. In Section V, proper basis functions by considering the edge boundary conditions are presented. Then, the resultant linear matrix is solved. The scattered field due to the equivalent magnetic current under a dielectric layer is then obtained in Section VI. In Section VII, the validity and efficiency of the proposed method for calculating the scattering fields of 3-D cracks under a dielectric layer is demonstrated by comparison with MoM and FEM results.

II. THE SCATTERING PROBLEM

Assume a dielectric filled rectangular crack of $a \times b \times c$ in an infinite ground plane is coated with a dielectric slab of height d and arbitrary permittivity and permeability of ε_2, μ_2 (Fig.1). This crack is illuminated by an arbitrary polarized plane wave. Using the surface equivalence principle, we can write the scattered fields in terms of the equivalent magnetic current distribution, $\vec{M}$ on the crack as:

$$\vec{E}^s = \left\langle {}_M\bar{\bar{G}}^e . \vec{M} \right\rangle,\ \vec{H}^s = \left\langle {}_M\bar{\bar{G}}^h . \vec{M} \right\rangle, \tag{1}$$

where ${}_M\bar{\bar{G}}^e$ and ${}_M\bar{\bar{G}}^h$ are magnetic dyadic Green's functions (DGFs). The ${}_M\bar{\bar{G}}^h$ is the Green's function for the magnetic field $\vec{H}$ generated by the magnetic current $\vec{M}$. In addition, the notation $\langle , \rangle$ means the integration of products of the two functions. The integral equation is constructed by enforcing the continuity of the total tangential magnetic field on the aperture of the crack under slab that separates region 2 from region 3. Thus, we have:

$$\vec{H}_{\tan}^{\text{region1}}(2\vec{M}, \vec{J}=0) + \vec{H}_{\tan}^{t} = \vec{H}_{\tan}^{\text{region2}}(-\vec{M}, \vec{J}=0), \tag{2}$$

where H^t is the total tangential magnetic field in the absence of the crack. Equation (2) is broken into a pair of coupled Fredlholm's integral equations of the first kind:

$$\begin{aligned} -H_x^t &= \iint_{s'} ({}_M^C G_{xx}^h + {}_M^D G_{xx}^h) M_x ds' + \iint_{s'} ({}_M^C G_{xy}^h + {}_M^D G_{xy}^h) M_y ds' \\ -H_y^t &= \iint_{s'} ({}_M^C G_{yx}^h + {}_M^D G_{yx}^h) M_x ds' + \iint_{s'} ({}_M^C G_{yy}^h + {}_M^D G_{yy}^h) M_y ds', \end{aligned} \tag{3}$$

where ${}_M^C G_{\alpha\beta=x,y}^h$ and ${}_M^D G_{\alpha\beta=x,y}^h$ are the magnetic green's functions of the crack and the grounded dielectric slab when the source and the observation points are both on the ground plane ($z=0$). Here, a direct approach is used to convert the electric or magnetic integral equations into a simple system of linear equation based on finite part sense integrals [19]. Initially, the behavior of the Green's functions is studied for extraction of the singular terms.

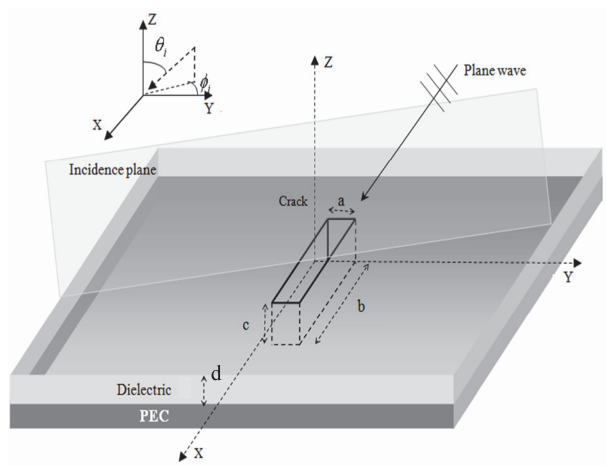

Fig. 1. Geometry of a narrow 3D-dimensional rectangular crack in an infinite ground plane underneath a dielectric layer.

III. DERIVATION OF DGFs

The most common method of deriving the DGFs is by means of Fourier transform and differential methods. Closed-form formulations of the DGFs for multilayered media using complex image method are reported in [21-29]. The well-known TL model is also used in addition to complex image method to find the spectral components of the stratified medium [22]. In Fig. 2, a magnetic current source is assumed on the infinite ground plane underneath the multilayered media. Figure 3 depicts the circuit equivalent transmission line model where the dielectric impedance is terminated by the free space wave impedance. The space domain Green's functions are obtained by applying the Sommerfeld transformation to the TL model as [26]:

$$G_{xx}(k_\rho, z, z'=0) = -\frac{\cos 2\phi}{\rho} S_1\left\{\frac{Y_t^h - Y_t^e}{k_\rho^2}\right\} - \sin^2\phi S_0\left\{Y_t^h\right\} - \cos^2\phi S_0\left\{Y_t^e\right\}, \tag{4}$$

$$G_{xy}(k_\rho, z, z'=0) = \frac{\sin 2\phi}{\rho} S_1\left\{\frac{Y_t^h - Y_t^e}{k_\rho^2}\right\} - \frac{1}{2}\sin 2\phi S_0\left\{Y_t^h - Y_t^e\right\}, \tag{5}$$

$$G_{yx}(k_\rho, z, z'=0) = G_{xy}(k_\rho, z, z'=0), \tag{6}$$

$$G_{yy}(k_\rho, z, z'=0) = \frac{\cos 2\phi}{\rho} S_1\left\{\frac{Y_t^h - Y_t^e}{k_\rho^2}\right\} - \sin^2\phi S_0\left\{Y_t^e\right\} - \cos^2\phi S_0\left\{Y_t^h\right\}, \tag{7}$$

where $\gamma_i = \sqrt{k_\rho^2 - \omega^2 \mu_i \varepsilon_i}$ and $k_\rho = \sqrt{k_x^2 + k_y^2}$ are cylindrical propagation constant and wave number, respectively. In the above equations, $S_n\{\ \}$ are the Sommerfeld integrals that are solved by the proper selection of branch cuts and integration paths [30].

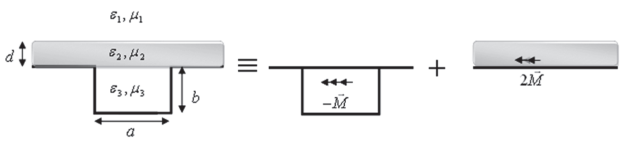

Fig. 2. The equivalence principle and image theory for a crack in an infinite ground plane.

Here, the spectral-domain Green's function is approximated by a pole-residue term plus an asymptotic function [26-28]. Thus,

$$\tilde{G}(k_\rho) \approx \sum_n a_n e^{-b_n k_\rho} + \sum_m \frac{2k_{\rho m}^p \, \mathrm{R}_m(k_{\rho m}^p)}{k_\rho^2 - (k_{\rho m}^p)^2}, \tag{8}$$

$\mathrm{R}_m(k_{\rho m}^p)$ represents the residues of $\tilde{G}$ at real poles $k_{\rho m}^p$. The Prony coefficients a_n and b_n are found by using GPOF and choosing the path C by avoiding the poles $k_\rho / k_1 = t\left[1 + j0.1e^{(1-t)}\right],\ 0 \le t \le 1.2k_{\max}/k_1$ shown in Fig. 4 [26]. In our case, the cracks are not only small but also close to the metal surface. Therefore, the lateral wave effects are small. Thus, on the conductor (z=0), we could use the approximation of DGFs. Utilizing Hankel transform,

$$\int_0^\infty e^{-\alpha k_\rho} J_n(k_\rho)(k_\rho)^{1-n} dk_\rho = \frac{n(\alpha^2+\rho^2)^{1/2} + (-1)^n \alpha}{\rho^n (\alpha^2+\rho^2)^{-n+3/2}}, \qquad n = 0,1. \tag{9}$$

Thus, $S_{0,1}$ in (4)-(7) are approximated as:

$$S_1 \approx -\frac{j}{2}\sum_m H_1(k_{\rho m}\rho) R_m + \frac{1}{2\pi}\sum_n a_n \frac{\sqrt{\rho^2 + b_n^2} - b_n}{\rho\sqrt{\rho^2 + b_n^2}}, \tag{10}$$

$$S_0 \approx -\frac{j}{2}\sum_m k_{\rho m} R_m H_0(k_{\rho i}\rho) + \frac{1}{2\pi}\sum_n \frac{a_n b_n}{\sqrt{(\rho^2 + b_n^2)^3}}. \tag{11}$$

Since the observation points are close to the source on the ground plane, the surface waves are dominant and the residues must be calculated precisely. The method of [31] is used for extraction of poles and calculation of residues.

For the computation of the Green's functions of the cavity, various approaches such as Ewald's method are available [32- 34]. Here, we used the approach of [34] for deriving the dyadic Green's functions of the cavity because the singular behavior is represented as a sum of infinite

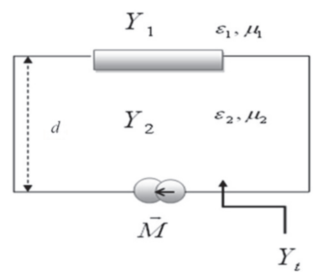

Fig. 3. Transmission line model of a magnetic source on a grounded slab.

harmonics. Since in many applications including NDT, the crack width is much smaller than the wavelength and the crack length, the DGFs are approximated by the lowest order mode of the crack [35]. Thus, the space domain Green's functions on the crack are [36]:

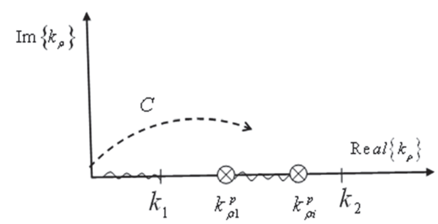

Fig. 4. The integration path in the k_ρ-plane for the sommerfeld integral.

$${}_M^C G_{xx}^h = D(k_3^2 - k_x^2)\sin k_x(x'-a)\sin k_x(x-a)\sum_{p=0}^{\infty} n_p \frac{\cos k_y(y'-b)\cos k_y(y-b)}{k_z.\tan k_z c}, \tag{12}$$

$${}_M^C G_{xy}^h = Dk_x \cos k_x(x'-a)\sin k_x(x-a)\sum_{p=1}^{\infty} k_y \frac{\sin k_y(y'-b)\cos k_y(y-b)}{k_z.\tan k_z c}, \tag{13}$$

$${}_M^C G_{yx}^h = Dk_x \sin k_x(x'-a)\cos k_x(x-a)\sum_{p=1}^{\infty} k_y \frac{\cos k_y(y'-b)\sin k_y(y-b)}{k_z.\tan k_z c}, \tag{14}$$

$${}_M^C G_{yy}^h = D\sum_{p=1}^{\infty} \frac{k_3^2 - k_y^2}{k_z.\tan k_z c}\sin k_y(y'-b)\sin k_y(y-b), \tag{15}$$

where $k_x = \frac{\pi}{2a}$, $k_y = \frac{p\pi}{2b}$, $k_z = \sqrt{k_3^2 - k_x^2 - k_y^2}$, $D = 2/(j\omega\mu_3 ab)$ and n_p is the Neumann's symbol(1 for *p=0* and 2 for *p >0*).

IV. SINGULARY EXTRACTION

The singularities in equations (4)-(7) are encountered when the observation point is on the source, *i.e.* $x = x'$ or $y = y'$ By expanding of the Hankel's functions around $y = y'$, display second-order hypersingularity and logarithmic singularity. Next, (4)-(7) are rearranged as:

$$ {}^{D}_{M}G^{h}_{xx} = \frac{f^{1}_{xx}(x,x')}{|x-x'|^{2}} + f^{2}_{xx}(x,x')\log|x-x'| + f^{3}_{xx}(x,x'), \tag{16}$$

$$ {}^{D}_{M}G^{h}_{xy} \approx {}^{D}_{M}G^{h}_{yx} \approx 0, \tag{17}$$

$$ {}^{D}_{M}G^{h}_{yy} = \frac{f^{1}_{yy}(x,x')}{|x-x'|^{2}} + f^{2}_{yy}(x,x')\log|x-x'| + f^{3}_{yy}(x,x'), \tag{18}$$

where $f^{1,2,3}$ are smooth functions obtained by the method of [6]. Note that the above procedure is repeated for all values of y and y' where $x = x'$.

The complete harmonic series of (12)-(15) either converge very slowly or diverge [6, 37]. Additionally, any truncation of the series creates a large error due to the miscalculation of the remainder of the series at $x = x'$ [6]. Therefore, the efficient approach of [37] is used to extract the singular terms of the harmonic series of (12)-(15). Considering a high enough number of modes (*i.e.,* $p>p_0$), the series coefficients are approximated as:

$$ \frac{1}{k_z.\tan k_z c} \cong \frac{1}{p} + o(p^{-3}), \quad \frac{k_y}{k_z.\tan k_z c} \cong 1 + o(p^{-2}), \quad \frac{k_3^2 - k_y^2}{k_z.\tan k_z c} \cong p + \frac{1}{p} + O(p^{-3}). \tag{19}$$

Finally, by substituting (19) in (12)-(15) and using the analytic simplifications of [6], the crack dyadic Green's functions are derived as:

$$ {}^{C}_{M}G^{h}_{xx} = D(k_3^2 - k_x^2)\sin k_x(x'-a)\sin k_x(x-a) \\ [\sum_{p=0}^{p_0} n_n \frac{\cos k_y(y'-b)\cos k_y(y-b)}{k_z.\tan k_z c} + g^{1}_{xx}\log|y-y'| + g^{2}_{xx}], \tag{20}$$

$$ {}^{C}_{M}G^{h}_{yx} \approx {}^{C}_{M}G^{h}_{xy} = Dk_x \cos k_x(x'-a)\sin k_x(x-a) \\ [\sum_{p=1}^{p_0} \frac{k_y}{k_z.\tan k_z c}\sin k_y(y'-b)\cos k_y(y-b) + \frac{g^{1}_{xy}}{|y-y'|} + g^{2}_{xy}], \tag{21}$$

$$ {}^{C}_{M}G^{h}_{yy} = D[\sum_{p=1}^{p_0} \frac{k_3^2 - k_y^2}{k_z.\tan k_z c}\sin k_y(y'-b)\sin k_y(y-b) + \frac{g^{1}_{yy}}{|y-y'|^{2}} + g^{2}_{yy}\log|y-y'| + g^{3}_{yy}], \tag{22}$$

where $g^{1,2,3}_{\alpha,\beta=x,y}$ are derivable nonsingular functions [6].

V. SOLUTION OF THE COUPLED INTEGRAL EQUATIONS

Direct integral equation solvers (DIES) straightforwardly solve the Integral equations with logarithmic or hypersingular kernels [38]. This method directly computes the finite part integral by numerical quadrature techniques that avoid the boundary singularities [19-20]. The magnetic currents at the edges of the crack are

$$ M_x(-a,y') = M(a,y) = M_y(x',-b) = M(x',b) = 0. \tag{23}$$

Please note that $M_x(x',b)$, $M_x(x',-b)$, $M_y(-a,y')$ and $M_y(a,y')$ are unknown magnetic currents on the crack and may tend to infinity at edges. By setting $s,s' = x,x'/a$ and $t,t' = y,y'/b$, the integral equation interval is transformed to $t,t',s,s' \in (-1,1)$. Next, the magnetic currents are approximated by finite series of products of two independent basic functions that satisfy the boundary conditions of (23). The first basis is a 'pulse' function and the other is a weighted Chebyshev polynomial of the second kind. Thus,

$$ M_x(s,t) \cong \sqrt{1-s^2}\sum_{m'=1}^{M}\sum_{n'=1}^{N} A_{m'n'}U_{m'-1}(s)P_{\Delta t_{n'}}(t-t_{n'}), \tag{24}$$

and

$$ M_y(s,t) \cong \sqrt{1-t^2}\sum_{m'=1}^{M}\sum_{n'=1}^{N} B_{m'n'}U_{n'-1}(t')P_{\Delta s_{m'}}(s-s_{m'}), \tag{25}$$

where $A_{m'n'}$ and $B_{m'n'}$ are unknown coefficients that must be calculated. P_Δ is the pulse basis functions of width $\Delta s_{m'}, \Delta t_{n'}$ where $\Delta s_{m'} = s_{m'} - s_{m'-1}\,(\Delta s_{m'} < 1)$, $\Delta s_{m'} = s_{m'} - s_{m'-1}\,(\Delta s_{m'} < 1)$. Additionally, $U_{m'}$ is the m[th] degree Chebyshev polynomial of the second kind. Using the zeros of $U_{m',n'}$, t_n and s_m, the surface of the crack is discretized to $M \times N$ non-equal elements. Hence,

$$ s_m = \cos\frac{m\pi}{M+1},\ m=1,...M \text{ and } t_n = \cos\frac{n\pi}{N+1},\ n=1,...N. \tag{26}$$

By substituting (24) and (25) in (3) and collocating at each t_n and s_m on the crack we have:

$$ \begin{cases} \frac{H_x(s_m,t_n)}{ab} = \sum_{n'=1}^{N}\sum_{m'=1}^{M} A_{m'n'}\left\langle K_{xx}(s_m,s'|t_n,t').O^{x}_{m'n'}(s',t')\right\rangle + \sum_{n'=1}^{N}\sum_{m'=1}^{M} B_{m'n'}\left\langle K_{xy}(s_m,s'|t_n,t').O^{y}_{m'n'}(s',t')\right\rangle \\ \frac{H_y(s_m,t_n)}{ab} = \sum_{n'=1}^{N}\sum_{m'=1}^{M} A_{m'n'}\left\langle K_{yx}(s_m,s'|t_n,t').O^{x}_{m'n'}(s',t')\right\rangle + \sum_{n'=1}^{N}\sum_{m'=1}^{M} B_{m'n'}\left\langle K_{yy}(s_m,s'|t_n,t').O^{y}_{m'n'}(s',t')\right\rangle \end{cases} \tag{27}$$

where $O^{x}_{m'n'}(s',t') = \sqrt{1-s^2}U_{m'-1}(s)P_{\Delta t_{n'}}(t-t_{n'})$ and $O^{y}_{m'n'}(s',t') = \sqrt{1-t^2}U_{n'-1}(t)P_{\Delta s_{m'}}(s-s_{m'})$. Subsequently, the coupled integral equation of (27) is represented in a linear system as:

$$ \begin{bmatrix} [H_x] \\ [H_y] \end{bmatrix} = \begin{bmatrix} [\langle K_{xx}, O^{x}_{m'n'}\rangle] & [\langle K_{xy}, O^{y}_{m'n'}\rangle] \\ [\langle K_{yx}, O^{x}_{m'n'}\rangle] & [\langle K_{yy}, O^{y}_{m'n'}\rangle] \end{bmatrix} \begin{bmatrix} [A] \\ [B] \end{bmatrix}, \tag{28}$$

where A and B are $1 \times MN$ unknown matrices that include unknown coefficients of (28) and are represented as $A = [\underbrace{A_{11},...A_{1N}}, \underbrace{A_{21},...A_{2N}}, ...\underbrace{A_{M1}...A_{MN}}]^T$ and

$B=[B_{11},...B_{1N},B_{21},...B_{2N},...,B_{M1}...B_{MN}]$. An arbitrary incident wave of Fig 1 can be decomposed into a parallel (E) and a perpendicular (H) Polarizations as:

$$\begin{cases} \vec{H}^i=\vec{\phi}e^{jk_1[(x\cos\varphi_i+y\sin\varphi_i)\sin\theta_i+z\cos\theta_i]} & H-Pol. \\ & \\ \vec{E}^i=\vec{\phi}e^{-jk_1[(x\cos\varphi_i+y\sin\varphi_i)\sin\theta_i+z\cos\theta_i]} & E-Pol. \end{cases} \quad \varphi_i\in[0,2\pi] \quad ,\ \theta_i\in[0,\pi/2], \tag{29}$$

where $k_1=2\pi/\lambda_0$ is the free space wave number and φ_i and θ_i are the incidence angles. The tangential magnetic field ($\vec{H}^t=\vec{H}_x\vec{x}+\vec{H}_y\vec{y}$) in the absence of the crack could be calculated by Fresnel's laws [39].

VI. FAR FIELD SCATTERING

Upon solving (3), the equivalent magnetic current on the crack is calculated and then, the far field due to this embedded source in the grounded slab is obtained [13, 40-41]. Following the approach of [41], approximate closed form solution of ${}^f_M\tilde{G}^H_\phi$ and ${}^f_M\tilde{G}^E_\phi$ are found by using the inverse Hankel transform. Thus:

$$r^2\left|(H,E)^s_\phi\right|^2=\left|{}^f_{M_x}G^{(E,H)}_\phi(\phi_o,\theta_o)P_x(\phi_o,\theta_o)+{}^f_{M_y}G^{(E,H)}_\phi(\phi_o,\theta_o)P_y(\phi_o,\theta_o)\right|, \tag{30}$$

where

$$P_x(\phi_o,\theta_o)=\pi ab\sum_{m'=1}^{M}\sum_{n'=1}^{N}A_{m'n'}m'j^{m'-1}\frac{J_{m'-1}(X)}{X}\Delta t_{n'}e^{jt_{n'}Y}, \tag{31}$$

$$P_y(\phi_o,\theta_o)=\pi ab\sum_{m'=1}^{M-1}\sum_{n'=1}^{N-1}B_{m'n'}\,n'\,j^{n'-1}\frac{J_{n'-1}(Y)}{Y}\Delta s_{m'}\,e^{js_{m'}X}. \tag{32}$$

In derivation of P_x and P_y the following mathematical relation is used.

$$\int_{-1}^{1}\sqrt{1-x^2}U_{m+1}(x)e^{\alpha x}dx=\pi(m+1)j^m\frac{J_m(\alpha x)}{\alpha x}. \tag{33}$$

The α th order Bessel function of the first kind is denoted by J_α and where $X=-k_1a\cos\phi_o\sin\theta_0$ and $Y=-k_1b\sin\phi_o\sin\theta_0$.

VII. RESULTS

Here, few numerical examples that demonstrate the validity of this approach are presented. Assuming $a=0.1\lambda,\ b=0.8\lambda,\ c=0.25\lambda,\ h=0.1\lambda,\ \varepsilon_2=3.2-0.1j$ and $\varepsilon_3=1$ in the configuration of Fig. 1, the calculated magnetic currents distribution $|M_x|$ and $|M_y|$ at the center of the crack (*x=0* and *y=0*) for $\phi_i=0^0$ and $\theta_i=45^0$ are depicted in Fig. 5 and Fig. 6 for parallel (E) and perpendicular (H) polarizations, respectively.

Then, the bistatic polarimetric radar cross sections ($\sigma^{bi}_{HH},\sigma^{bi}_{VV},\sigma^{bi}_{VH}$) at a constant observation elevation angle $\theta_o=45^0$ are compared with the fully numerical approaches of FEM and MoM for a crack with the dielectric cover (WD) and without the dielectric cover (WoD) as shown in Fig. 7.

The dielectric cover causes σ^{bi}_{VV} to rise slightly; however, the other bistatic radar cross sections decrease by 8 dB. Figure 8 represents the same results for a constant observation azimuth angle $\phi_o=0^0$. σ^{bi}_{VV} is almost constant while the bistatic cross polarizations increase and σ^{bi}_{HH} decreases compared to uncovered crack. As shown, the results are in a good agreement with full numerical approaches.

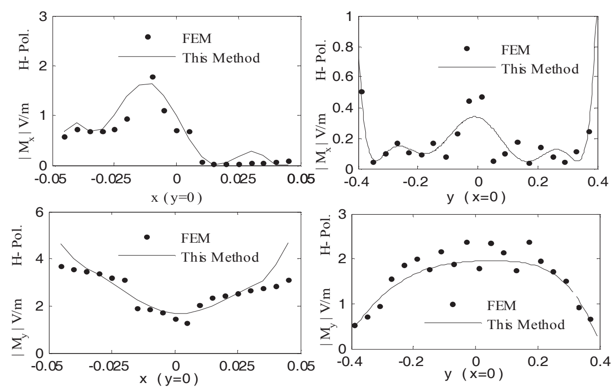

Fig. 5. Comparison between magnetic current of DIES and FEM for the crack of Fig. 1 with $a=0.1\lambda,\ b=0.8\lambda,\ c=0.25\lambda,\ h=0.1\lambda,\ \varepsilon_2=3.2-0.1j,\ \varepsilon_3=1$ for horizontal polarizations (H-Polarization) when $\phi_i=0^o$ and $\theta_i=45^o$.

In the above examples, *M* = 17 and *N*=35 with the dielectric cover and *M*=13 and *N*=29 without the dielectric cover generated accurate results. When the frequency, the permittivity, or the length of the crack increase, the Hankel's function arguments and the crack propagating modes increase as well and thus, the number of collocation points should increase for adequate accuracy. On the other hand, due to the highly oscillatory integrals, an inappropriate high number of *M* and *N* reduce the calculation efficiency without any sensible improvement [42-43].

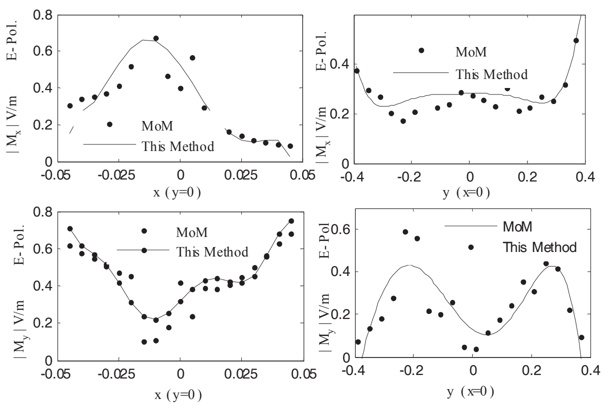

Fig. 6. Comparison between magnetic current of DIES and MoM for the crack of Fig. 1 with: $a=0.1\lambda, b=0.8\lambda, c=0.25\lambda, h=0.1\lambda, \varepsilon_2=3.2-0.1j$ and $\varepsilon_3=1$ for vertical polarizations (E-Polarization) at $\phi_i=0^o$ and $\theta_i=45^o$.

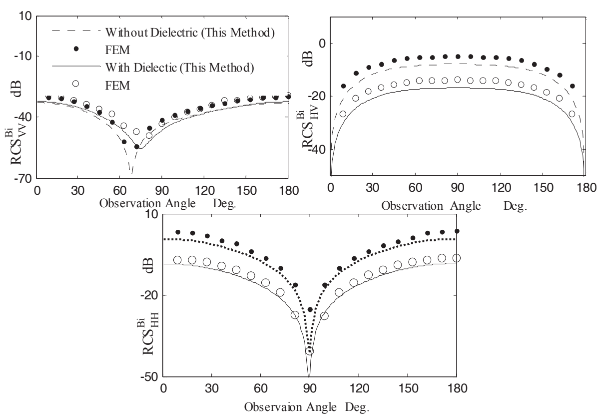

Fig. 7. Bistatic radar cross sections (RCS^{bi}) of the crack in Fig. 1 at various observation angles ϕ_o with $a=0.1\lambda, b=0.8\lambda, c=0.25\lambda, h=0.1\lambda, \varepsilon_2=3.2-0.1j$ and $\varepsilon_3=1$ at $\phi_i=0^o$.

A rapid convergence of these integrals is very important in minimizing CPU time. For integrals that include Bessel and harmonic functions, an extended Levin's collocation method of [43] is used that approximates the oscillatory integrals. On a 2 GHz Pentium4 PC of 1G RAM, the computation time of FEM (HFSS), MoM (FEKO) and our method (DIES) for the dielectric covered crack of Fig. 6 are 38.136, 32.751, and 18.225 minutes, respectively. Please note that the calculation of oscillatory integrals in (3) is the most time consuming computation of DIES.

Examination of the results shows that the crack dielectric cover alters the RCS signature significantly even for thin layers. Surface waves are also a contributing factor in RCS reduction where the dielectric layer acts as a waveguide that traps the wave and thus reduces the scattered energy.

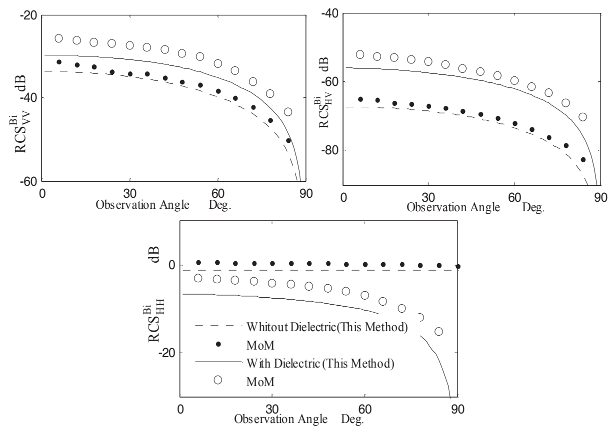

Fig. 8. RCS^{bi} of the crack in Fig. 1 at various observation angles θ_0 with $a=0.1\lambda, b=0.8\lambda, c=0.25\lambda, h=0.1\lambda, \varepsilon_2=3.2-0.1j$ and $\varepsilon_3=1$ at $\phi_i=0^o$ and $\theta_i=45^o$.

Table1: Some material with their dielectric constants

material	permittivity
Air	1
Polystyrene	2.2
Epoxy	3.5
Glass,Mica	6
GaAs	13

Figure 9 depicts the variations of RCS^{bi} for various dielectric constants of Table 1 for $a=0.2\lambda$, $b=1\lambda$, $c=0.25\lambda, h=0.1\lambda$ and $\varepsilon_3=1$ at $\phi_i=30^0$ and $\theta_i=30^0$. By increasing the dielectric constant, RCS^{bi} drops down at first and then slowly increases due to an increase in the electrical thickness of the substrate that excites additional surface wave modes. Thus, an increase in the excitation energy in the crack causes RCS^{bi} to rise. On the contrary, as the dielectric constant increases to a large value such as $\varepsilon_2=13$, the high reflectivity at the air-dielectric interface reduces the RCS^{bi}. As the dielectric constant increases, the minimum RCS^{bi} as a function of elevation angle shifts to the left. In addition for $\varepsilon_2 \le 6$, the RCS^{bi} is smoother and the scattering beam width widens for high permittivity. Referring to Fig. 9, the energy density in the forward scattering region ($180^o < \phi_o < 360^o$) is higher than other directions due to specula reflection.

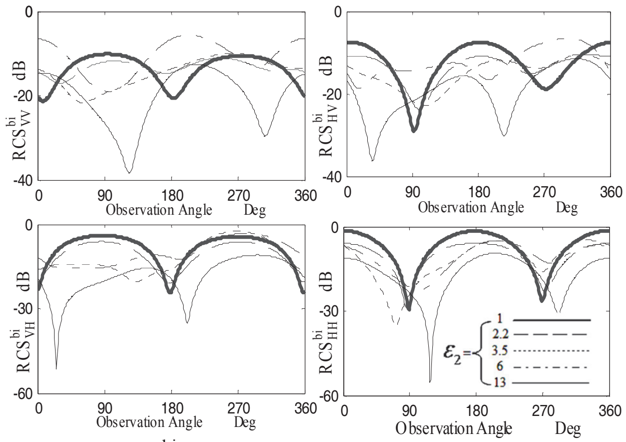

Fig. 9. RCS^{bi} of the crack in Fig. 1 versus observation angles ϕ_o or materials of table 1 where $a=0.2\lambda, b=1\lambda, c=0.25\lambda, h=0.1\lambda$ and $\varepsilon_3=1$ at $\phi_i=30^o$ and $\theta_i=30^o$.

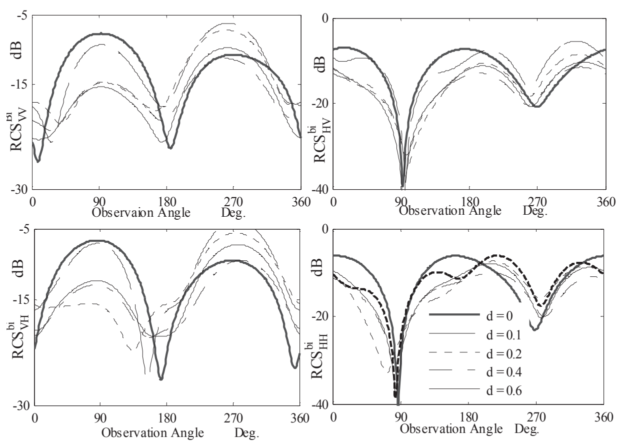

Fig. 10. RCS^{bi} of the crack in Fig. 1 versus observation angles ϕ_o for different dielectric thicknesses where $a=0.2\lambda$, $b=1\lambda$, $c=0.25\lambda, h=0.1\lambda$, $\varepsilon_2=2.5-j0.05$ and $\varepsilon_3=1$ at $\phi_i=45^o$ and $\theta_i=30^o$.

In conclusion, the dielectric constant of the layer does not have a monotonic effect on polarimetric scattering cross sections. In order to study the influence of the substrate thickness, a crack with $a=0.2\lambda$, $b=1\lambda$, $c=0.25\lambda$, $\varepsilon_2=2.5-j0.05$, $\varepsilon_3=1$ and $h=0, 0.1\lambda, 0.2\lambda, 0.4\lambda, 0.6\lambda$ is illuminated at $\phi_i=45^o$ and $\theta_i=30^o$ and the RCS^{bi} variations are shown in Fig. 10.

As dielectric thickness increases, the RCS^{bi} in the forward scattering region increases while in the exciting source region ($0^o<\phi_o<180^o$) decreases. The RCS^{bi} dips for co-polarization at $\phi_o=180^o$ and $\phi_o=360^o$ and for cross-polarization at $\phi_0=90^o$ and $\phi_o=270^o$ are thickness independent. Similar to the influence of the dielectric constant, the dielectric thickness effect is not monotonic as well, noting that the surface waves are more prevalent in this case.

VIII. CONCLUSION

Most approaches in the literature use the electric and the magnetic potential integral equations to solve electromagnetic problems. Here, a direct field method is developed to solve the magnetic integral equations of a three dimensional rectangular crack in a grounded slab covered by a dielectric layer. This invertible solution is in demand in inverse scattering and NDT applications. The approach efficiently solves the integral equation by extraction of the hyper-singular terms and then descritizing the integral equation. The two-dimensional integrals include strong singularities that are approximated by ad hoc quadrature rules leading to a linear system of equations. In addition, the calculation of the oscillatory integrals is expedited by Levin's method that is developed in applied mathematics. A good agreement is observed with MoM and FEM solutions that are full numerical and non-invertible. In addition, the sensitivity of the RCS^{bi} to the permittivity and thickness of overlaying layer is investigated. In general, the dielectric layer alters the polarimetric scattering signatures of a crack in a non-monotonic manner.

Appendix: SOME QUADRATURE RULES

In equations (22-24) and (26-28), hypersingular, logarithmic and ordinary integral are present. An expression for the hypersingular integrals is in the form of [44]:

$$\int_{-1}^{1}(1-t^2)^{1/2}/|s-t|^2 f(t)dt = \pi\sum_{j=1}^{M+1} w_j(s) f(s_j), \tag{A.1}$$

where $f(t)$ is a given regular function and M is a integer. Here,

$$s_j = \cos j\pi/(M+2)\,,\ (j=1,2,...,M+1), \tag{A.2}$$

$$w_j(s) = -\frac{2}{M+2}\sum_{n=0}^{M}(n+1)\sin(\frac{j\pi}{M+2})\sin(\frac{(n+1)j\pi}{M+2})U_n(s) \qquad (A.3)$$

$$\int_{-1}^{1} U_m(t)(1-t^2)^{1/2} / \left|s-t\right| dt = -\pi T_{m+1}(s) \qquad m \geq 0 \qquad (A.4)$$

and T_m is the m^{th} degree Chebyshev polynomial of the first kind.

REFERENCES

[1] N. Ida, *Microwave NDT,* vol. 10, Department of Electrical Engineering, University of Akron, Ohio, 1992.

[2] R. Khalaj-Amineh, M. Ravan, S. H. H. Sadeghi, and R. Moini, "Removal of Probe Lift-Off Effects on Crack Detection and Sizing in Metals by the AC Field Measurement Technique," *IEEE Transactions on Magnetics*, vol. 44, no. 8, pp. 2066-2073, Aug. 2008.

[3] C. Huber, H. Abiri, S. Ganchev, and R. Zoughi, "Modeling of Surface Hairline-Crack Detection in Metals under Coatings using an Open-Ended Rectangular Waveguide," *IEEE Trans. on Microwave Theory and Techniques*. vol. 45, no. 11, pp. 2049-57, Nov. 1997.

[4] F. Mazlumi, S. H. H. Sadeghi, and R. Moini, "Interaction of Rectangular Open-Ended Waveguides with Surface Tilted Long Cracks in Metals," *IEEE Transactions on Instrumentation & Measurement*, vol. 55, no. 6, pp. 2191-2197, Dec. 2006.

[5] F. Deek, and M. El-Shenawee, "Microwave Detection of Cracks in Buried Pipes using the Complex Frequency Technique," *Applied Computational Electromagnetic Society (ACES) Journal*, vol. 25, no.10, pp. 894-902, Oct. 2010.

[6] M. Bozorgi, A. Tavakoli, G. Monegato, S. H. H. Sadeghi, and R. Moini, "Backscattering from a Two Dimensional Rectangular Crack Using FIE," *IEEE Trans. Antennas Propagat*., vol. 58, no. 2, pp. 552-564, Feb. 2010.

[7] C. M. Knop and G. I. Cohn, "Radiation from an Aperture in a Coated Plane," *Radio Science Journal of Research*, vol. GSD, pp. 363-378, Apr. 1964.

[8] C. P. Wu, "Integral Equation Solutions for the Radiation from a Waveguide through a Dielectric Slab," *IEEE Trans. Antennas Propagat*., vol.17, no. 6, pp. 733-739, Nov. 1969.

[9] R. D. Nevels, "An Analysis of a Two-Dimensional Dielectric Covered Corrugated Antenna Feed Horn," *IEEE Trans. Antennas Propagat*., vol. 32, no. 8, pp. 877-880, Aug. 1984.

[10] R. D. Nevels and C. M. Butler, "Electromagnetic Scattering by a Surface Wave from a Notch in a Ground Plane Covered by a Dielectric Slab," *J. Appl. Phys.,* vol. 52, no. 5, pp. 3145-3147, May 1981.

[11] J. W. Lee, H. J. Eom, K. H. Park, and W. J. Chun, " TM-Wave Radiation from Grooves in a Dielectric- Covered Ground Plane," *IEEE Trans. Antennas Propagat*., vol. 49, no. 1, pp. 104-105, Jan. 2001.

[12] T. F. Eibert and V. Hansen, "On the Calculation of Potential Integrals for Linear Source Distributions on Triangular Domains," *IEEE Trans. Antennas Propagat.*, vol. 43, no. 12, 1499–1502, December 1995.

[13] Yl¨a-Oijala, P. and M. Taskinen, "Calculation of CFIE Impedance Matrix Elements with RWG and n×RWG Functions," *IEEE Trans. Antennas Propagat.*, vol. 51, no. 8, 1837–1846, August 2003.

[14] H. A. Sabbagh, R. K. Murphy, E. H. Sabbagh, J. C. Aldrin, J. S. Knopp, and M. P. Blodgett, "The Joy of Computing with Volume Integrals: Validation and Performance Comparison," *Applied Computational Electromagnetic Society (ACES) Journal*, vol. 25, no. 9, pp. 731-737, September 2010.

[15] J. Hadmard, Lectures on Cauchy's Problem in Linear Partial Differential Equations. Yale University Press, Yale, 1932.

[16] A. M. Lerer and A. G. Schuchinsky, "Full-Wave Analysis of Three-Dimensional Planar Structures," *IEEE Trans. Microwave Theory and Techniques*, vol. 41, no. 11, pp. 2002-2014, 1993.

[17] A. I. Nosich, "The Method of Analytical Regularization in Wave Scattering and Eigenvalue Problems: Foundations and Review of Solutions," *IEEE Antennas and Propagation Magazine*, vol. 41, pp. 34-49, June 1999.

[18] G. Fikioris, "A Note on the Method of Analytical Regularization," *IEEE Transactions on Antennas and Progagation Magazine*, vol. 43, pp. 34-40, April 2001.

[19] G. Monegato, "Definitions, Properties, and Applications of Finite Part Integrals," *J. Comput. Appl. Math*., vol. 229, p. 425, 2009.

[20] G. Monegato, "Numerical Evaluation of Hypersingular Integrals," *J. Comput. Appl. Math.,* vol. 50, pp. 9-31, May 1994.

[21] W. C. Chew, *Waves and Fields in Inhomogeneous Media*, Van. Nostrand Reinhold, New York, 1990.

[22] Ylä-Oijala, P. and M. Taskinen, "Efficient Formulation of Closed Form Green's Functions for General Electric and Magnetic Sources in Multilayered Media," *IEEE Trans. Antennas and Propagation*, vol. 51, no. 8, pp. 2106-2115, 2003.

[23] K. A. Michalski and J. R. Mosig, "Multilayered Media Green's Functions in Integral Equation Formulations," *IEEE Trans Antennas. Propagat,*, vol. 45, no. 3, pp. 508-519, March 1997.

[24] J. Bernal, F. Medina, R. R. Boix, and M. Horno, "Fast Full-Wave Analysis of Multistrip Transmission Lines on MPIE and Complex Image Theory," *IEEE Trans. Microw. Theory Tech.*, vol. 48, no. 3, pp. 445–452, Mar. 2000.

[25] M. I. Aksun and G. Dural, "Clarification of Issues on Closed-Form Green's Functions in Stratified Media *IEEE Transactions on Antennas and Propagation*, vol. 53, no. 11, pp. 3644-3653, Nov. 2005.

[26] R. R. Boix, F. Mesa, and F. Medina, "Application of Total Least Squares to the Derivation of Closed-Form Green's Functions for Planar Layered Media," *IEEE Trans. Microw. Theory Tech.*, vol. 55, no. 2, pp. 268-280, Feb. 2007.

[27] M. T. Yuan, T. L. Sarkar, and Salazar-Palma, "A Discrete Complex Image Method from the Closed-Form Green's Functions in Multilayered Media," *IEEE Trans. Microw. Theory Tech.*, vol. 54, no. 3, pp. 1025-1032, 2006.

[28] J. R. Mosig and Alvarez-Melcon, "Green's Functions in Lossy-Layered Media: Integration Along the Imaginary Axis and Asymptotic Behavior," *IEEE Trans. Antennas Propagat.*, vol. 51, pp. 3200-3208, Dec. 2003.

[29] A. Dreher, "A New Approach to Dyadic Green's Function in Spectral Domain," *IEEE Trans. Antennas Propagat.*, vol. 43, pp. 1297-1302, Nov. 1995.

[30] K. A. Michalski, " Extrapolation Methods for Sommerfeld Integral Tails," *IEEE Trans. Antennas Propagat.*, vol. 46, no. 10, pp. 1405-14182, Oct. 1998.

[31] M. Zhang, L. W. Li, and Y. F. Tian, "An Efficient Approach for Extracting Poles of Green's Functions in General Multilayered Media," *IEEE Trans. Antennas Propagat.*, vol. 56, no. 1, pp. 269-273, Jan. 2008.

[32] D. I. Wu and D. C. Cheng, "**A** Hybrid Representation of the Green's Function in an Overmoded Rectangular Cavity," *IEEE Trans. Antennas Propagat.,* vol. 36, no. 9, pp. 1334-1342, Sep. 1988.

[33] F. Capolino, D. R. Wilton, and W. A. Johnson, "Efficient Computation of the 2D Green's Function for 1D Periodic Arrays Using the Ewald Method,"*IEEE Trans. Antennas Propagat.*, vol. 53, no. 9, pp. 2977-2984, Sept. 2005.

[34] M.-J. Park, J. Park, and S. Nam, "Efficient Calculation of the Green's Function for the Rectangular Cavity," *IEEE Microwave and Guided Wave Letters*, vol. 8, no. 3, March 1998, pp. 124-126.

[35] K. Barkashli and J. L. Volakis," Scattering from Narrow Rectangular Filled Grooves," *IEEE Trans. Antennas Propagat*., vol. AP-39, no.10, pp. 804-810, June 1991.

[36] K. Y. Chow and K. W. Leung, "Theory and Experiment of the Cavity-Backed Slot-Excited Dielectric Resonator Antenna," *IEEE Trans. Electromag. Compat.*, vol. 42, no. 3, pp. 290-297, Aug. 2000.

[37] G. Monegato, R. Orta, and R. Tascone, "A Fast Method for the Solution of a Hypersingular Integral Equation Arising in a Waveguide Scattering Problem," *Int. J. Numer. Methods Eng.* vol. 67, no. 2, pp. 272-297, July 2006.

[38] Y. Chen, "Fast Direct Solver for the Lippmann-Schwinger Integral Equation," *Adv. Comput. Math*., vol. 16, pp. 175-190, 2002.

[39] C. A. Balanis, *Antenna Theory, Analysis and Design*, 3rd Ed., John Wiley & Sons, Hoboken, NJ, 2005.

[40] B. Stockbroeckx and A. Vander Vorst, "Asymptotic Green's Function of a Surface

Magnetic Current Element on a Perfect Electric Conductor Plane Covered by a Lossy Dielectric Substrate," *IEEE Trans. Antennas Propagat*., vol. 47, no. 2, pp. 309-316, February 1999.

[41] B. Wu and L. Tsang, "Fast Computation of Layered Medium Green's Functions of Multilayers and Lossy Media using Fast All Modes Method and Numerical Modified Steepest-Descent Path Method," *IEEE Trans. Microw. Theory Tech.*, vol. 56, pp. 1446–1454, Jun. 2008.

[42] S. Xiang, "Numerical Analysis of a Fast Integration Method for Highly Oscillatory Functions," *BIT Numerical Mathmetics*, vol. 47, pp. 469-482, June, 2007.

[43] A. Molabahrami and F. Khani, "Numerical Solutions of Highly Oscillatory Integrals," *Appl. Math. Comput*., vol. 98, no. 2, pp. 657-664, 2008.

[44] M. Abramowitz and I. A. Stegun, *Handbook of Mathematical functions with formulas, Graphs, and Mathematical Tables,* vol. 55 of Applied Mathematics series, Department of commerce, National Bureau of Standards, 1972.

Mehdi bozorgi was born in Isfahan, Iran on September 4, 1977. He received B.S. and M.S degrees in Electrical Engineering from the Kashan University and the Amirkabir University of technology, respectively. In 2011, He received Ph.D. degree in Electrical Engineering at Amirkabir university of Technology, Tehran, Iran. His research field of interest is scattering of electromagnetic waves, electromagnetic nondestructive testing and optics.

Ahad Tavakoli was born in Tehran, Iran, on March 8, 1959. He received B.S. and M.S. degrees from the University of Kansas, Lawrence, and the Ph.D. degree from the University of Michigan, Ann Arbor, all in Electrical Engineering, in 1982, 1984, and 1991, respectively. In 1991, he joined the Amirkabir University of Technology, Tehran, Iran, where he is currently a Professor in the Department of Electrical Engineering. His research interests include EMC, scattering of electromagnetic waves and microstrip antennas.